Acta Crystallographica Section D
**Biological Crystallography**
ISSN 0907-4449

# Structure of the sortase AcSrtC-1 from *Actinomyces oris*

**Karina Persson**

Department of Odontology, Umeå University, SE-901 87 Umeå, Sweden

Correspondence e-mail: karina.persson@odont.umu.se

Received 14 December 2010
Accepted 3 February 2011

**PDB Reference:** AcSrtC-1, 2xwg.

The crystal structure of the sortase AcSrtC-1 from the oral microorganism *Actinomyces oris* has been determined to 2.4 Å resolution. AcSrtC-1 is a cysteine transpeptidase that is responsible for the formation of fimbriae by the polymerization of a shaft protein. Similar to other pili-associated sortases, the AcSrtC-1 active site is protected by a flexible lid. The asymmetric unit contains five AcSrtC-1 molecules and their catalytic Cys–His–Arg triads are trapped in two different conformations. It is also shown that the thermostability of the enzyme is increased by the presence of calcium.

## 1. Introduction

Together with oral streptococci, the oral bacterium *Actinomyces oris* (formerly *A. naeslundii*; Henssge *et al.*, 2009) is among the first colonizers of the oral cavity. As such, it is important in the formation of the oral biofilm (dental plaque). The bacterium is Gram-positive and can express two forms of fimbriae: type 1 and type 2 (Cisar *et al.*, 1988). Type 1 fimbriae mediate the adhesion of the bacteria to salivary proline-rich proteins that coat the surface of the tooth enamel (Gibbons *et al.*, 1988), which is an important step in initiating growth of the oral biofilm. Type 2 fimbriae contribute to biofilm formation by binding to carbohydrate structures on early-colonizing streptococci and host cells (Palmer *et al.*, 2003). The major shaft proteins of type 1 and type 2 fimbriae are encoded by the genes *fimP* and *fimA*, respectively. They are encoded in separate operons and both are located between a putative adhesin and a fimbriae-specific sortase (Chen *et al.*, 2007; Yeung *et al.*, 1998) that is responsible for the covalent polymerization of the shaft protein. Sortases are cysteine transpeptidases and can be divided into two classes, housekeeping sortases (SrtA) and pilus sortases (SrtC), which catalyze related but distinct reactions. Housekeeping sortases are membrane-associated transpeptidases that recognize and cleave proteins between the threonine and the glycine of the peptidoglycan anchor motif LP*X*TG in the C-terminal end (Ton-That *et al.*, 2004). During the reaction, the threonine of the surface protein becomes covalently bound to the nucleophilic cysteine of the sortase, after which the protein is transferred to the peptidoglycan of the cell wall. The polymerization of fimbriae (or pili) requires specific sortases that catalyze a similar reaction by cleaving the fimbrial shaft protein at its LP*X*TG motif and linking the threonine to a conserved lysine of another subunit. This results in a stepwise polymerization of the fimbriae. The cores of the housekeeping sortases and the fimbriae/pili-specific sortases are structurally conserved (Manzano *et al.*, 2009; Neiers *et al.*, 2009). However, while the housekeeping sortases have an openly accessible active site, the fimbriae/pili-associated sortases have a flexible

**Table 1**
Data-collection, refinement and model-quality statistics for AcSrtC-1.

Values in parentheses are for the highest resolution shell.

| | |
|---|---|
| Data processing | |
| Space group | $P2_12_12_1$ |
| Unit-cell parameters (Å) | $a$ = 104.07, $b$ = 108.23, $c$ = 143.20 |
| Wavelength (Å) | 0.979 |
| Resolution (Å) | 45.5–2.4 (2.53–2.40) |
| Total reflections | 365089 (42433) |
| Unique reflections | 62240 (8451) |
| $\langle I/\sigma(I)\rangle$ | 16.6 (4.2) |
| $R_{\rm merge}$† (%) | 7.8 (35.8) |
| Completeness (%) | 97.5 (91.9) |
| Multiplicity | 5.9 (5.0) |
| Refinement | |
| No. of reflections in working set | 58993 |
| No. of reflections in test set | 3245 |
| $R_{\rm work}/R_{\rm free}$‡ (%) | 20.5/24.4 |
| Wilson $B$ factor (Å$^2$) | 44.3 |
| Average $B$ factor (Å$^2$) | |
| Protein | 44.9 |
| Water | 36.1 |
| $Ca^{2+}$ | 63.0 |
| No. of protein atoms | 6957 |
| No. of metal ions | 4 |
| No. of water molecules | 220 |
| R.m.s.d. from ideal | |
| Bond lengths (Å) | 0.011 |
| Bond angles (°) | 1.412 |
| Ramachandran plot (%) | |
| Most favoured | 86.3 |
| Allowed | 11.9 |
| Generously allowed | 1.1 |
| Disallowed | 0.9 |

† $R_{\rm merge} = \sum_{hkl}\sum_i |I_i(hkl) - \langle I(hkl)\rangle|/\sum_{hkl}\sum_i I_i(hkl)$, where $I_i(hkl)$ is the intensity of the $i$th observation of reflection $hkl$ and $\langle I(hkl)\rangle$ is the average over of all observations of reflection $hkl$. ‡ $R_{\rm work} = \sum_{hkl}\big||F_{\rm obs}| - |F_{\rm calc}|\big|/\sum_{hkl}|F_{\rm obs}|$, where $F_{\rm obs}$ and $F_{\rm calc}$ are the observed and calculated structure-factor amplitudes, respectively. $R_{\rm free}$ is $R_{\rm work}$ calculated using 5% of the data omitted from refinement.

lid that covers the active site (Manzano *et al.*, 2009). This is believed to be part of a mechanism that is used by the enzyme to select the proper shaft protein for polymerization. The anchoring of many adhesins on Gram-positive bacteria is sortase-dependent. Therefore, these enzymes are attractive targets for the development of novel anti-infectives and every sortase structure will add to the optimization of more efficient drug candidates. In this study, the crystal structure of the *A. oris* sortase AcSrtC-1, the enzyme that catalyses the polymerization of the FimP shaft protein, was determined. Furthermore, a thermal shift assay showed that calcium plays an important role in stabilizing the enzyme.

## 2. Materials and methods

### 2.1. Cloning

The *srtc-1* gene encoding residues 80–288 of the protein was amplified from genomic DNA of *A. oris* strain T14V (GenBank accession code ABG47035). The preparation of the genomic DNA has been described previously (Hallberg *et al.*, 1998). PCR primers were designed to include the part of the protein located between the predicted TM helices (residues 59–81 and 308–330). The forward primer was 5′-TTTTT**CC-ATGG**CGACCCAGCACAACAA-3′ and the reverse primer was 5′-AAAAA**GGTACC**TCACGTGGGGTCCATTGGGA-C-3′ (restriction sites are shown in bold). The PCR product was digested with *Acc*65I and *Nco*I and ligated into the equivalent sites of the pET-M11 expression vector (kindly provided by G. Stier, EMBL, Germany). The final construct encodes $His_6$-PMSDYDIPTTENLYFQGA–AcSrtC-$1_{80–288}$. The plasmids were transformed into *Escherichia coli* DH5$\alpha$ and subsequent colonies were selected for on kanamycin plates. The positive clones were verified by DNA sequencing.

### 2.2. Overexpression and purification

The protein was overexpressed in *E. coli* BL21 (DE3) at 310 K in Luria broth supplemented with 50 µg ml$^{-1}$ kanamycin. When the cultures reached an $OD_{600}$ of 0.6, the temperature was lowered to 303 K and expression was induced with 0.4 m*M* IPTG, after which the cultures were grown for an additional 5 h. The cells were harvested by centrifugation at 5300*g* and the pellets were frozen at 193 K. The cell pellets were resuspended in 20 m*M* Tris–HCl pH 7.5, 150 m*M* NaCl and 10 m*M* imidazole supplemented with EDTA-free protease-inhibitor cocktail (Roche). The suspension was lysed by sonication on ice and cellular debris was removed by centrifugation at 39 000*g* for 60 min. The supernatant was loaded onto a column packed with Ni–NTA agarose (Qiagen). The protein was washed in 20 m*M* Tris–HCl pH 7.5, 150 m*M* NaCl and 20 m*M* imidazole and eluted with 20 m*M* Tris–HCl pH 7.5, 150 m*M* NaCl and 300 m*M* imidazole. The buffer was exchanged to 20 m*M* Tris–HCl pH 7.5, 150 m*M* NaCl, 0.5 m*M* EDTA and 1 m*M* DTT. The protein was further purified by size-exclusion chromatography using a HiLoad 16/60 Superdex 200 prep-grade column (Amersham Biosciences). The protein purity was judged by SDS–PAGE.

### 2.3. Crystallization and data collection

The purified protein was concentrated to 110 mg ml$^{-1}$ in 20 m*M* Tris–HCl pH 7.5, 0.5 m*M* EDTA and 1 m*M* DTT using an Amicon Ultra centrifugal filter device (Millipore). Initial crystallization trials were performed by the sitting-drop vapour-diffusion method in a 96-well MRC crystallization plate (Molecular Dimensions) using a Mosquito pipetting robot (TTP LabTech). Untreated protein and protein treated with 1%(*w*/*w*) $\alpha$-chymotrypsin were used in the setups. *In situ* proteolysis was performed as a means of trimming off flexible parts to facilitate crystal growth as described previously (Dong *et al.*, 2007). In brief, $\alpha$-chymotrypsin stored at 2 mg ml$^{-1}$ in 100 m*M* Tris pH 7.8, 2 m*M* $CaCl_2$ was added to the sortase to a final ratio of 1%(*w*/*w*) immediately before crystallization. In both setups the sortase was diluted to a final concentration of 30 mg ml$^{-1}$ in 20 m*M* HEPES pH 7.5. Droplets consisting of 0.1 µl protein solution were mixed with an equal volume of reservoir solution using screens from Hampton Research (Crystal Screen HT) and Molecular Dimensions (PACT). Crystals were obtained from 1.9 *M* sodium formate and 1.9 *M* potassium formate at 291 K. Crystals were soaked for 30 s in mother-liquor solution supplemented with 20% glycerol

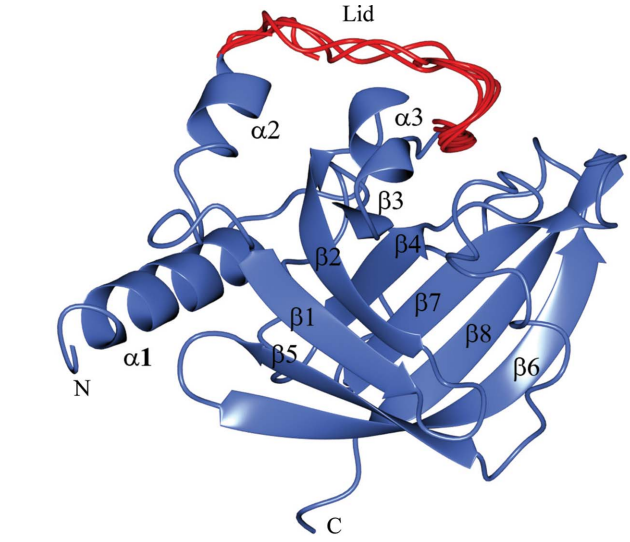


(*a*)

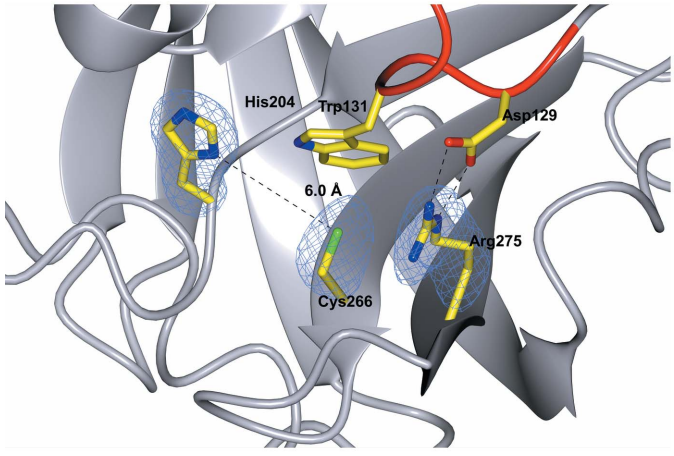


(*b*)

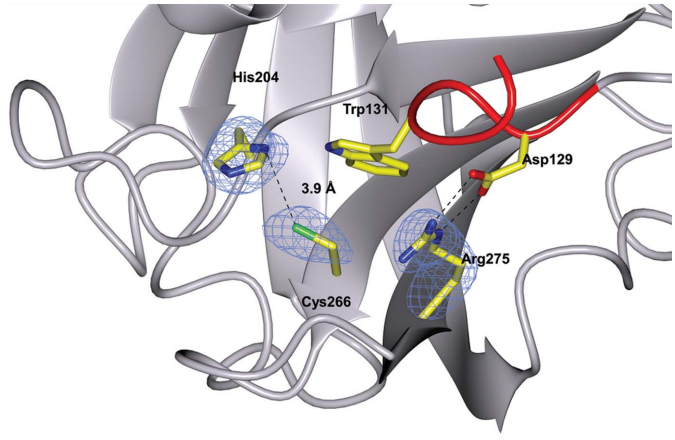


(*c*)

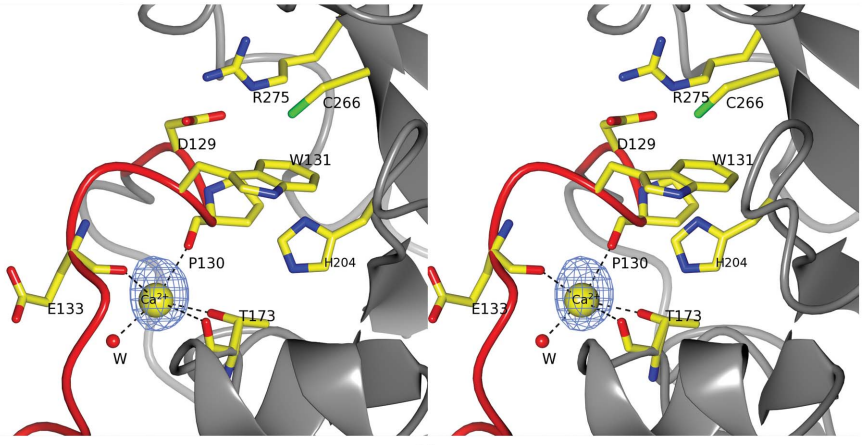


(*d*)

before being flash-cooled in liquid nitrogen and stored until data collection.

Diffraction data were collected to 2.4 Å resolution using a MAR Mosaic 225 detector on beamline I911-3 at MAX-lab, Lund, Sweden. Diffraction images were processed with *MOSFLM* (Leslie, 2006) and scaled with *SCALA* from the *CCP*4 program suite (Collaborative Computational Project, Number 4, 1994). Relevant processing statistics are summarized in Table 1.

### 2.4. Analysis of crystal contents

The purified protein solution and the crystal contents were analysed by MALDI–TOF mass spectrometry. Purified protein was diluted to 2 mg ml$^{-1}$ in 0.1%(*v*/*v*) TFA and AcSrtC-1 crystals obtained from the $\alpha$-chymotrypsin-treated protein were briefly washed in water and dissolved in 0.1% TFA before analysis.

**Figure 1**
The crystal structure of AcSrtC-1. (*a*) AcSrtC-1 folds into a $\beta$-barrel with three helices positioned on one side. A flexible lid, depicted in red, covers the active site. The lids from all molecules (*A*–*E*) have been included in order to illustrate their flexibility. (*b*) The active-site residues can adopt different conformations. The Cys266 nucleophile forms a sulfur–aromatic interaction with Trp131 located in the active-site lid. The catalytic Arg275 is anchored to Asp129 in the lid. The active site His204 is located 6.0 Å away from the nucleophile. Side chains are depicted as stick models. The cysteine, histidine and arginine are represented in a simulated-annealing OMIT $F_o - F_c$ electron-density map contoured at 3$\sigma$. (*c*) This figure was prepared as in (*b*) but the cysteine and histidine have adopted different conformations and are located 3.9 Å apart from each other. The conformation of the arginine has not changed. (*d*) A putative $Ca^{2+}$-binding site is located between the flexible lid and the coil between $\alpha$3 and $\beta$2. The ion is coordinated by Pro130 (O) and Glu133 (O) as well as by Thr173 (OG and O) and a water molecule. Side chains are depicted as stick models. The calcium ion is shown as a yellow sphere in a simulated-annealing OMIT $F_o - F_c$ electron-density map contoured at 3$\sigma$. The figure is shown in stereo.

### 2.5. Thermal shift assay

AcSrtC-1 was screened for stabilizing metal ions using the Thermofluor method (Ericsson *et al.*, 2006). In brief, solutions of 2× Sypro Orange (Molecular Probes), 30 m*M* HEPES pH 7.5, 5 m*M* salt (NaCl, KCl, LiCl, $CaCl_2$, $MgCl_2$ and $MnCl_2$) and 0.6 µg protein in a total volume of 25 µl were mixed in 0.1 ml PCR tubes and heated in a qPCR detection system (Rotor-Gene 6000, Corbett Life Science) from 301 to 353 K in increments of 0.5 K. Changes in fluorescence were monitored and the melting temperature ($T_m$) was determined by calculating the derivative of the midpoint of the protein-unfolding transition. The experiment was performed in triplicate.

### 2.6. Structure determination and refinement

The structure of AcSrtC-1 was solved by molecular replacement using the core residues (71–205) of the *Streptococcus pneumoniae* sortase (PDB code 2w1j; Manzano *et al.*, 2008) as a model. Five molecules were found in the asymmetric unit using *MOLREP* (Vagin & Teplyakov, 2010), corresponding to a Matthews coefficient of 4.0 Å$^3$ Da$^{-1}$ (69.5% solvent content; Matthews, 1968).

The model was manually rebuilt and refined using iterative cycles of *Coot* (Emsley *et al.*, 2010) and *phenix.refine* (Afonine *et al.*, 2005). The first round of refinement included simulated annealing starting at 5000 K. Fivefold NCS was applied throughout the refinement. The NCS groups were automatically defined by *phenix.refine* and included all residues except 133–136. In the last rounds of refinement translation–libration–screw (Winn *et al.*, 2001) refinement was used, treating each molecule as an individual TLS group. The quality of the model was analyzed with *WHATCHECK* (Hooft *et al.*, 1996). Refinement statistics are summarized in Table 1. Figures were drawn with *CCP*4*MG* (Potterton *et al.*, 2004). The X-ray coordinates and structure factors have been deposited in the Protein Data Bank under accession code 2xwg.

## 3. Results and discussion

### 3.1. Crystallization and analysis of crystal contents

Crystals of AcSrtC-1 were only obtained from protein that had been treated with α-chymotrypsin immediately before crystallization setup. MALDI–TOF analysis verified that the protein in the crystal had a mass of 20 410 Da, whereas the untreated protein had a mass of 26 073 Da. (The calculated mass of the protein construct is 26 100 Da; Supplementary Fig. S1[1]). The crystals belonged to space group $P2_12_12_1$, with unit-cell parameters $a$ = 104.1, $b$ = 108.2, $c$ = 143.2 Å.

### 3.2. Overall structure of AcSrtC-1

The final model of AcSrtC-1 is comprised of five molecules (*A*–*E*) in the asymmetric unit of the crystal (residues 105–285 in molecule *A*, 103–287 in molecule *B*, 107–285 in molecule *C*, 102–285 in molecule *D* and 105–285 in molecule *E*). The overall structure is comprised of an eight-stranded β-barrel flanked by three helices on one side (Fig. 1*a*). This fold is in agreement with previously solved sortase structures (Neiers *et al.*, 2009; Manzano *et al.*, 2008; Weiner *et al.*, 2010; Suree *et al.*, 2009; Zong *et al.*, 2004; Race *et al.*, 2009; Zhang *et al.*, 2004; Ilangovan *et al.*, 2001).

The largest variation between the five molecules is observed in residues 132–139. In molecules *A*, *B* and *D* the main chain and most side chains could be modelled. In molecules *C* and *E* the quality of the electron density was poorer, which resulted in chain breaks at residues 134–136 and 135–138, respectively. This flexible stretch constitutes part of a lid that covers the active site.

A small movement is also seen in the turn (residues 207–210) that connects β4 to the following $3_{10}$-helix. This turn is also located in connection with the active site. The five molecules in the asymmetric unit form two dimers (*A* with *D* and *C* with *E*) and one monomer (*B*). Dimer formation is also observed in the crystal structures of the pili sortases SrtC-1 and SrtC-3 from *S. pneumoniae* (Manzano *et al.*, 2008). The dimers seen in these structures are not believed to be the functional forms since these proteins are reported to elute as monomers during gel filtration. AcSrtC-1 also elutes as a monomer and analysis using the *PISA* server (Krissinel & Henrick, 2007) predicted that the dimer interactions in the crystal would be too weak to be biologically stable: $\Delta G^{\rm diss} = -6.3$ and $-8.0$ kJ mol$^{-1}$ for the *AD* and the *CE* dimers, respectively. However, light-scattering analysis of the protein indicates that the protein is a dimer in solution [the measured diameter is 6.7 nm, which is closer to the calculated diameter of a dimer (6.4 nm) than of a monomer (4.8 nm)]. The monomer in the asymmetric unit does not form any dimer interactions by crystallographic symmetry and its structure does not deviate much from those of molecules involved in dimer formation. The root-mean-square deviations (r.m.s.d.s) between the five different chains range from 0.5 to 0.9 Å calculated on all $C^\alpha$ atoms.

### 3.3. Active site

The active site is located at the top of the β-barrel. Like both pilus-associated and housekeeping sortases, AcSrtC-1 contains a conserved Cys–His–Arg triad (Figs. 1*b* and 1*c*). The active site is covered by a lid (residues 129–139) with the sequence DPWLESQRPDT. The active-site lid is a feature that is common to pilus sortases but is not present in housekeeping sortases, which have a more exposed active site. The C-terminal end of the lid (residues 132–139) constitutes the most flexible part of the structure, whereas the first part (residues 129–131) is very rigid. The nucleophile Cys266 is located at the centre of the active site at the C-terminus of β7. It is positioned under the lid and in four of the five molecules it forms sulfur–aromatic interactions with the lid residue Trp131. The carboxylate group of another lid residue, Asp129, locks the side chain of the triad residue Arg275 (β8) in place with

[1] Supplementary material has been deposited in the IUCr electronic archive (Reference: HM5095). Services for accessing this material are described at the back of the journal.

two hydrogen bonds. The histidine (His204) is located in the turn after $\beta$4, 6 Å from the Cys266 SG atom. The catalytic mechanism, and especially the role of the histidine, has been the focus of intense debate. It has been proposed that the histidine activates the cysteine by deprotonation and that together they form a thiolate–imidazolium ion (Ton-That *et al.*, 2002). However, the distance between the two residues is too long in all of the NMR and crystal structures to support such a model. However, it was shown that in the active form of SrtA from *Staphylococcus aureus* both the His and the Cys are charged. Nonetheless, only a small fraction (0.06%) of the molecules are present in their active form prior to binding the substrate (Frankel *et al.*, 2005).

In one of the five AcSrtC-1 molecules (the *C* chain), Cys266 and His204 have adopted altered conformations in which the Cys SG and His ND1 atoms are located only 3.9 Å apart. This rotamer of Cys266 is similar to one of the cysteine conformations of the *S. pyogenes* pili sortases (PDB codes 2w1j and 3g66; Manzano *et al.*, 2008; Neiers *et al.*, 2009) that exhibit dual conformations. His204 is rotated closer to both Cys266 and Trp131, an arrangement that is unique to AcSrtC-1. The conformational change is induced by crystal packing that forces His204 from its original position. This may be an artefact that is solely induced by crystal packing, but it still gives indications that the cysteine may indeed be activated by a thiolate–imidazolium ion interaction facilitated by small changes in side-chain conformations. This packing does not cause any difference in the conformation of any other active-site residue. The crystal-packing-induced conformational change of His204 opens speculation that the sortase is activated by the binding of its substrate, the FimP shaft protein.

NMR studies on SrtA from *S. aureus* in complex with an LPAT substrate (Suree *et al.*, 2009) indicate that the active-site histidine also functions as an acid that protonates the amide leaving group. The conserved arginine on the opposite side of the nucleophile is proposed to play a key role in the reaction by stabilizing the position of the leucine and proline residues of the sorting signal. As pointed out by Suree *et al.* (2009), the lid residues Pro-Trp of SrtC-1 and Pro-Phe of SrtC-3 of *S. pneumoniae* (Manzano *et al.*, 2008) are located in the same position as Pro-Ala of the LPAT sorting sequence in complexed SrtA. Similarly, the lid residues Asp129, Pro130 and Trp131 of AcSrtC-1 overlap with the LPAT peptide. This strengthens the hypothesis that the lid mimics the LP*X*TG sorting sequence and is used to fill and protect the active site when the proper substrate is absent.


**Figure 2**
Comparison of pilus sortases. Superposition of AcSrtC-1 in red and *S. pneumoniae* SrtC-1 in blue (PDB code 2w1j). The N- and C-termini are labelled, as well as the location of the active site. The figure is shown in stereo.

### 3.4. Calcium dependence

In *S. aureus* SrtA $Ca^{2+}$ has been shown to increase the enzymatic activity by modulating the structure and dynamics of an active-site loop, inducing a binding-competent cleft (Naik *et al.*, 2006). Although the SrtA loop is not comparable with the lid described for AcSrtC-1, it is possible that the accessibility of the AcSrtC-1 active site is also controlled by the presence of metal ions. In the crystal structure of AcSrtC-1 strong density peaks are located near the lids of molecules *A* and *C*. The density peak is stronger in molecule *A*, which is in agreement with the fact that the lid in molecule *A* is the most ordered of all five molecules in the asymmetric unit owing to its involvement in crystal packing with a neighbouring molecule. A $Ca^{2+}$ ion has been modelled in this position, coordinated by Pro130 (O) and Glu133 (O) in the lid as well as by Thr173 (OG and O) in the turn between $\beta$2 and $\alpha$3 and a water molecule (Fig. 1*d*). In two of the monomers (*A* and *B*) $Ca^{2+}$ ions were also modelled more distal to the active site, between $\alpha$1 and $\alpha$2, coordinated by Asp150 (OD1), Glu111 (OE1 and OE2) and His147 (O). Since the protein was crystallized in the presence of only trace amounts of $Ca^{2+}$ (a final concentration of 0.3 m*M* $CaCl_2$ from the addition of $\alpha$-chymotrypsin), the $Ca^{2+}$ binding was further investigated by soaking crystals with 5–10 m*M* $CaCl_2$ for 1 h before data collection. Nonetheless, $Ca^{2+}$ was only observed in the same positions as described above, probably as a consequence of the crystallization conditions and crystal packing (data not shown).

To investigate whether AcSrtC-1 is stabilized by any metal, thermally induced melting assays were performed in the presence of NaCl, KCl, LiCl, $CaCl_2$, $MgCl_2$ and $MnCl_2$ using the Thermofluor method (Ericsson *et al.*, 2006). The results showed that calcium was the metal that most significantly stabilized the sortase, shifting the $T_m$ from 321 to 327 K. The only other metal that had any effect was manganese, which resulted in a single peak at 324 K (Fig. S2). The present crystal structure, together with the results of the thermal shift assay, supports a model in which the $Ca^{2+}$ ion holds the active-site lid in a closed form, thereby protecting the catalytic residues from exposure when there is no sorting signal. For binding to occur the $Ca^{2+}$ ion would need to dissociate and the lid would need to open. This regulatory function may be dissimilar to the calcium-dependence of the housekeeping sortases, in which the metal ion is used to arrange an open binding pocket that is prepared to accommodate the substrate. This putative difference in calcium-dependent

regulation may reflect the high substrate specificity of the fimbrial sortase *versus* the need for the housekeeping sortases to accommodate a variety of substrates.

### 3.5. Comparison of sortase structures

The core part of AcSrtC-1, the eight-stranded $\beta$-barrel, is related to those of housekeeping sortases such as SrtA (Zong *et al.*, 2004). However, AcSrtC-1 is flanked by helices on one side, with the region located between the first two helices forming a lid that covers the active site. This feature is not present in SrtA, which has a more open active site. Instead, AcSrtC-1 is structurally very similar to the pili sortases SrtC-1 and SrtC-3 from *S. pneumoniae*. Except for the fact that the first helix in the *S. pneumoniae* structures is not present in the *A. oris* crystal structure, the major differences are found in the lid over the active site and the region that follows until the first $\beta$-strand. This region is a coil followed by an $\alpha$-helix in AcSrtC-1, whereas the equivalent region of *S. pneumoniae* pilus sortase SrtC-1 is folded like a long coil (Manzano *et al.*, 2008; Fig. 2). This region also deviates in structure when comparing the different *S. pneumonie* sortases that are known to date. I hypothesize that this region next to the active site constitutes a recognition channel designed to bind and distinguish between substrate proteins.

## 4. Conclusions

The crystal structure of the *A. oris* sortase revealed that this enzyme is very similar in structure to other sortases. The largest deviations are seen in the loop over the active site and in a putative substrate-binding groove. The AcSrtC-1 crystal structure demonstrates that the active-site residues can adopt a different conformation. The role of calcium in stabilizing the protein has also been demonstrated. Further structural studies of the complex between the fimbrial shaft protein and the sortase will be needed in order to fully understand the mechanism behind recognition and polymerization of the fimbriae. Since sortases are considered to be promising targets for the design of novel antibiotics against Gram-positive bacteria such structures would be very valuable.

I am grateful for access to beamline I911-3 at MAX-lab, Lund, Sweden and the support of the beamline scientists. I thank Gunter Stier, EMBL, Germany for cloning vectors. The mass spectroscopy was performed by Thomas Kieselbach at Umeå Protein Analysis Facility, Umeå University. This work was supported by the Swedish Research Council and foundations at Umeå University.

## References

Afonine, P. V., Grosse-Kunstleve, R. W. & Adams, P. D. (2005). *CCP4 Newsl.* **42**, contribution 8.
Chen, P., Cisar, J. O., Hess, S., Ho, J. T. & Leung, K. P. (2007). *Infect. Immun.* **75**, 4181–4185.
Cisar, J. O., Vatter, A. E., Clark, W. B., Curl, S. H., Hurst-Calderone, S. & Sandberg, A. L. (1988). *Infect. Immun.* **56**, 2984–2989.
Collaborative Computational Project, Number 4 (1994). *Acta Cryst.* D**50**, 760–763.
Dong, A. *et al.* (2007). *Nature Methods*, **4**, 1019–1021.
Emsley, P., Lohkamp, B., Scott, W. G. & Cowtan, K. (2010). *Acta Cryst.* D**66**, 486–501.
Ericsson, U. B., Hallberg, B. M., Detitta, G. T., Dekker, N. & Nordlund, P. (2006). *Anal. Biochem.* **357**, 289–298.
Frankel, B. A., Kruger, R. G., Robinson, D. E., Kelleher, N. L. & McCafferty, D. G. (2005). *Biochemistry*, **44**, 11188–11200.
Gibbons, R. J., Hay, D. I., Cisar, J. O. & Clark, W. B. (1988). *Infect. Immun.* **56**, 2990–2993.
Hallberg, K., Holm, C., Ohman, U. & Strömberg, N. (1998). *Infect. Immun.* **66**, 4403–4410.
Henssge, U., Do, T., Radford, D. R., Gilbert, S. C., Clark, D. & Beighton, D. (2009). *Int. J. Syst. Evol. Microbiol.* **59**, 509–516.
Hooft, R. W., Vriend, G., Sander, C. & Abola, E. E. (1996). *Nature (London)*, **381**, 272.
Ilangovan, U., Ton-That, H., Iwahara, J., Schneewind, O. & Clubb, R. T. (2001). *Proc. Natl Acad. Sci. USA*, **98**, 6056–6061.
Krissinel, E. & Henrick, K. (2007). *J. Mol. Biol.* **372**, 774–797.
Leslie, A. G. W. (2006). *Acta Cryst.* D**62**, 48–57.
Manzano, C., Contreras-Martel, C., El Mortaji, L., Izoré, T., Fenel, D., Vernet, T., Schoehn, G., Di Guilmi, A. M. & Dessen, A. (2008). *Structure*, **16**, 1838–1848.
Manzano, C., Izoré, T., Job, V., Di Guilmi, A. M. & Dessen, A. (2009). *Biochemistry*, **48**, 10549–10557.
Matthews, B. W. (1968). *J. Mol. Biol.* **33**, 491–497.
Naik, M. T., Suree, N., Ilangovan, U., Liew, C. K., Thieu, W., Campbell, D. O., Clemens, J. J., Jung, M. E. & Clubb, R. T. (2006). *J. Biol. Chem.* **281**, 1817–1826.
Neiers, F., Madhurantakam, C., Fälker, S., Manzano, C., Dessen, A., Normark, S., Henriques-Normark, B. & Achour, A. (2009). *J. Mol. Biol.* **393**, 704–716.
Palmer, R. J., Gordon, S. M., Cisar, J. O. & Kolenbrander, P. E. (2003). *J. Bacteriol.* **185**, 3400–3409.
Potterton, L., McNicholas, S., Krissinel, E., Gruber, J., Cowtan, K., Emsley, P., Murshudov, G. N., Cohen, S., Perrakis, A. & Noble, M. (2004). *Acta Cryst.* D**60**, 2288–2294.
Race, P. R., Bentley, M. L., Melvin, J. A., Crow, A., Hughes, R. K., Smith, W. D., Sessions, R. B., Kehoe, M. A., McCafferty, D. G. & Banfield, M. J. (2009). *J. Biol. Chem.* **284**, 6924–6933.
Suree, N., Liew, C. K., Villareal, V. A., Thieu, W., Fadeev, E. A., Clemens, J. J., Jung, M. E. & Clubb, R. T. (2009). *J. Biol. Chem.* **284**, 24465–24477.
Ton-That, H., Marraffini, L. A. & Schneewind, O. (2004). *Biochim. Biophys. Acta*, **1694**, 269–278.
Ton-That, H., Mazmanian, S. K., Alksne, L. & Schneewind, O. (2002). *J. Biol. Chem.* **277**, 7447–7452.
Vagin, A. & Teplyakov, A. (2010). *Acta Cryst.* D**66**, 22–25.
Weiner, E. M., Robson, S., Marohn, M. & Clubb, R. T. (2010). *J. Biol. Chem.* **285**, 23433–23443.
Winn, M. D., Isupov, M. N. & Murshudov, G. N. (2001). *Acta Cryst.* D**57**, 122–133.
Yeung, M. K., Donkersloot, J. A., Cisar, J. O. & Ragsdale, P. A. (1998). *Infect. Immun.* **66**, 1482–1491.
Zhang, R., Wu, R., Joachimiak, G., Mazmanian, S. K., Missiakas, D. M., Gornicki, P., Schneewind, O. & Joachimiak, A. (2004). *Structure*, **12**, 1147–1156.
Zong, Y., Bice, T. W., Ton-That, H., Schneewind, O. & Narayana, S. V. (2004). *J. Biol. Chem.* **279**, 31383–31389.